



# 1% > 100% : High-Efficiency Visual Adapter with Complex Linear Projection Optimization

Dongshuo Yin<sup>1</sup> Xue Yang<sup>2</sup> Deng-Ping Fan<sup>3</sup> Shi-Min Hu<sup>1</sup>

## Abstract

Deploying vision foundation models typically relies on efficient adaptation strategies, whereas conventional full fine-tuning suffers from prohibitive costs and low efficiency. While delta-tuning has proven effective in boosting the performance and efficiency of LLMs during adaptation, its advantages cannot be directly transferred to the fine-tuning pipeline of vision foundation models. To push the boundaries of adaptation efficiency for vision tasks, we propose an adapter with **Complex Linear Projection Optimization (CoLin)**. For architecture, we design a novel low-rank complex adapter that introduces only about 1% parameters to the backbone. For efficiency, we theoretically prove that low-rank composite matrices suffer from severe convergence issues during training, and address this challenge with a tailored loss. Extensive experiments on object detection, segmentation, image classification, and rotated object detection (remote sensing scenario) demonstrate that CoLin outperforms both full fine-tuning and classical delta-tuning approaches with merely 1% parameters for the first time, providing a novel and efficient solution for deployment of vision foundation models. We release the code on <https://github.com/DongshuoYin/CoLin>.

## 1. Introduction

Explosive growth of visual (Awais et al., 2025) and multi-modal (Li et al., 2025b) foundation models is spearheading an AI paradigm shift. Endowed with universal visual representation capabilities from large-scale pre-training (Du et al., 2022), these models demonstrate strong generalization

<sup>1</sup>BNRist, Department of Computer Science and Technology, Tsinghua University, Beijing, China <sup>2</sup>School of Automation and Intelligent Sensing, Shanghai Jiao Tong University, Shanghai, China

<sup>3</sup>Nankai International Advanced Research Institute (Shenzhen Fujian) & SLAI, Shenzhen, China.

Preprint. February 12, 2026.

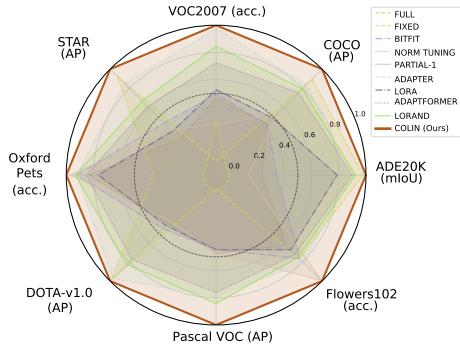


**Figure 1. Performance radar.** The proposed method outperforms full fine-tuning and typical delta-tuning approaches (based on Swin-B/L) on 8 visual tasks by fine-tuning **only about 1%** new params for the first time. This parameter efficiency advantage can be further enhanced on larger foundation models. The maximum on each axis represents the best performance of each dataset.

on core tasks (e.g., segmentation, detection) and empower high-stakes domains including autonomous driving (Gao et al., 2025), remote sensing (Yin et al., 2025b; Hu et al., 2024b;a), and medical imaging (Dutt et al., 2024). The distribution shift between pre-trained tasks and downstream tasks makes model adaptation a linchpin for real-world deployment. While full fine-tuning aligns task performance, it incurs prohibitive computational and storage costs and risks catastrophic forgetting. Delta-tuning (Han et al., 2024; Yu et al., 2024) enables lightweight adaptation by freezing backbones and optimizing only a small parameter subset—has emerged as a research focus. Efficient visual model adaptation is thus pivotal to foundation model deployment. In visual tasks, how to outperform full fine-tuning while updating the minimal number of parameters is a research question of significant theoretical and practical importance.

Recent delta-tuning methods in computer vision can be broadly divided into three families: reparameterization, adapter-based approaches, and partial fine-tuning. Reparameterization methods, such as the LoRA series (Hu et al., 2022), have shown impressive gains in large language models, but these benefits do not easily carry over to visual foundation models. Partial-tuning only updates certain components of the foundation model (such as normalization layers (Giannou et al., 2023), biases (Ben Zaken et al., 2022), or the

final few transformer blocks (Yosinski et al., 2014)), which often falls short of full fine-tuning in terms of performance (Yin et al., 2024). Adapter-based methods (Houlsby et al., 2019), while adding some inference overhead, generally yield more competitive results compared to the other two strategies. Original adapters consist of two linear layers: an up-projection and a down-projection. Together, these layers account for most of the adapter’s parameter, and their transfer efficiency is crucial for downstream task performance (Yin et al., 2023). However, existing art has not systematically analyzed or optimized linear projection layers for visual recognition tasks, limiting the efficiency ceiling of adapters in both vision tasks and even multimodal tasks.

To further improve the efficiency and performance of adapters for visual tasks, we conduct an in-depth analysis and optimization of the linear layers within the adapter architecture. First, we propose a multi-branch low-rank adapter structure based on a sophisticated sharing mechanism. Inspired by Mixture-of-Experts (MoE) designs, we replace the original monolithic projection matrix with a sum of multiple low-rank matrices of the same size. This design enhances the robustness of the projection matrix while significantly reducing the number of newly introduced parameters. Building on this, we introduce branch sharing and kernel matrix sharing mechanisms to further decrease the parameter footprint and improve the consistency of the adapter’s visual feature understanding. Compared to full fine-tuning, our approach reduces the number of parameters by more than 98%. Second, we observe that this design can lead to significant inefficiency during training. To investigate the factors affecting efficiency, we derive and prove, using matrix-theoretic arguments (Franklin, 2000), that the low-rank composite matrices suffer from gradient direction entanglement during backpropagation. Based on this theoretical insight, we introduce a necessary orthogonal loss during training and optimize the parameter initialization strategy to mitigate the impact of inefficient transfer. We perform extensive experiments to validate the effectiveness of our proposed method. Results (Figure 1) on object detection, instance segmentation, semantic segmentation, image classification, and rotated object detection tasks demonstrate that CoLin outperforms full fine-tuning and classical delta-tuning methods on both natural image and remote sensing scenarios. The contributions can be summarized as follows:

- We propose a multi-branch low-rank adapter architecture built on a sophisticated sharing mechanism, which significantly reduces the parameter and improves the transfer efficiency of visual features.
- Using matrix-theoretic principles, we prove the existence of an inefficiency issue in low-rank composite matrices during gradient backpropagation and introduce an orthogonal loss to mitigate the adverse effects

of inefficient gradient transfer.

- Comprehensive results on object detection, instance segmentation, semantic segmentation, image classification and rotated object detection demonstrate that the proposed method consistently outperforms both full fine-tuning and classical delta-tuning approaches with only about 1% new params across all these scenarios.

## 2. Related Work

### 2.1. Delta-tuning

Delta-tuning has been widely adopted across large language models, vision foundation models, and multimodal large models due to its parameter-efficiency and impressive performance. In natural language processing, LoRA (Hu et al., 2022) achieves strong performance with low-rank matrices. Adapter (Houlsby et al., 2019) insert bottleneck structures into the backbone to facilitate domain transfer, while prompt tuning optimizes model outputs by modifying the input distribution. In the vision domain, visual prompt tuning (Jia et al., 2022) treats additional learnable patches as prompts for fine-tuning. AdaptFormer (Chen et al., 2022) adds scalable bottleneck structures in skip connections to improve adaptation, and DAPE (Xia et al., 2025) employs a two-stage fine-tuning strategy for video editing. In multimodal tasks, DoRA (Liu et al., 2024) extends LoRA by optimizing both magnitude and direction, leading to better performance on text and video tasks. LoRASculpt (Liang et al., 2025) mitigates catastrophic forgetting in multimodal fine-tuning through LoRA pruning. Overall, delta-tuning not only significantly reduces the number of trainable parameters but also amplifies the advantages of pre-trained models in terms of performance, continual learning, and domain adaptation.

### 2.2. Adapter Optimization

Adapter-based methods have numerous variants, several of which have demonstrated impressive results in visual tasks. Appendix D presents the mathematical process of the adapter-tuning. Polyhistor (Liu et al., 2022) introduces a novel insertion strategy for multi-task learning. Adapter-Drop (Rücklé et al., 2021) dynamically removes lower-layer adapters during training to reduce computational overhead. LoRand (Yin et al., 2023) is the first work to apply adapter tuning to dense prediction tasks in vision. E<sup>3</sup>VA (Yin et al., 2024) proposes an adapter highway for visual tasks, effectively lowering training costs. ST-Adapter (Pan et al., 2022) extends adapter-based adaptation to image-to-video tasks by incorporating depthwise 3D convolutions. Compafter (Karimi Mahabadi et al., 2021) leverages Kronecker products to reduce the parameter count of adapters. The linear layers in adapters constitute the primary source of their parameter overhead. To date, existing work has not yet

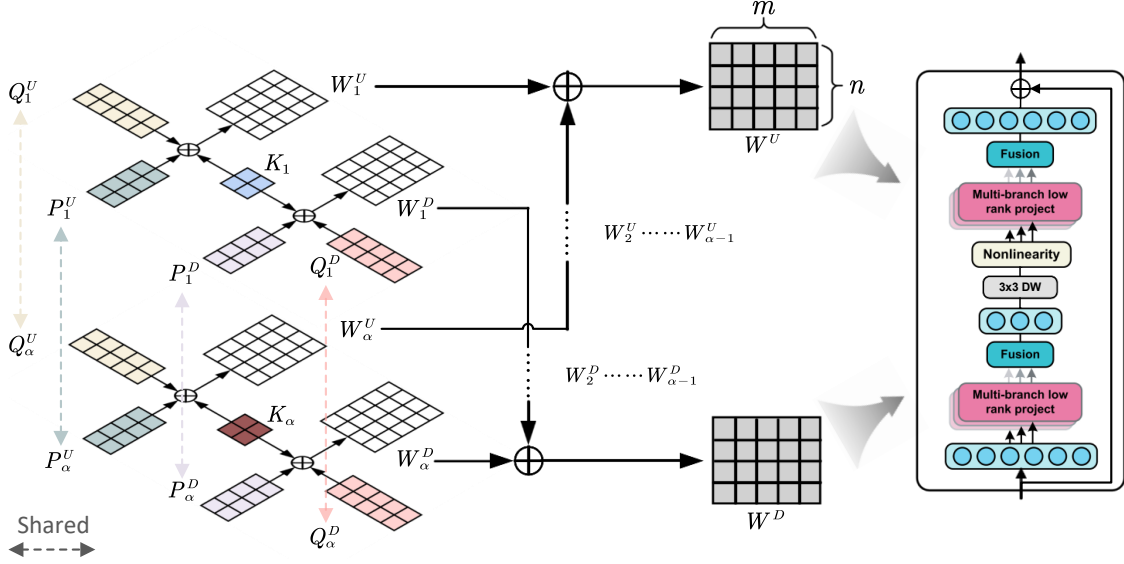


**Figure 2. Module schematic.** The down-projection  $W^D$  and up-projection  $W^U$  matrices are the summation of  $\alpha$  branches  $W_1^D(W_1^U) \dots W_\alpha^D(W_\alpha^U)$ .  $K_i$  in  $i$ -th branch is shared between  $W_i^D$  and  $W_i^U$ . All  $P$  and  $Q$  are shared among branches. All  $K_i$  are trainable, and all the  $W$  matrices are calculated. A single depth-wise (DW) convolution layer is added before GeLU.

provided theoretical analysis or dedicated optimization for the linear layers of visual adapters in vision tasks.

### 3. Methods

#### 3.1. Multi-branch Low-rank Projection

##### 3.1.1. STANDARD ADAPTER LINEAR PROJECTION

Before introducing the proposed method, we first review the existing adapter structure. Conventional adapters are bottleneck structures containing a down-projection, an up-projection, and a non-linear activation function. Besides, adapters ensure the robustness of the model by adding residual (He et al., 2016) structures. Adapter layer can be formulated as follows:

$$A^l = U^l (GeLU (D^l (x))) + x, \quad (1)$$

where  $U^l$  and  $D^l$  represent the up and down projections in the  $l$ -th adapter layer, and GeLU is the activation function. It is clear that the parameters in adapter come from the projections. The projection process can be written as:

$$y = Wx + b, \quad (2)$$

which means most adapter parameters are in  $W$ .

##### 3.1.2. LOW-RANK LINEAR PROJECTION

To reduce the adapter parameters, we propose a projection matrix construction method based on multi-branch design, which can effectively reduce the parameters of  $W$ . Figure 2 shows the simplified structure of CoLin. Here we approximate not a specific matrix  $W$  but an ideal matrix  $W_{best}$  that

can transform the feature space of the pre-trained model into new tasks by heuristic learning. The approximation matrix  $\hat{W}$  has the same size as  $W$ , but the low-rank design makes  $\hat{W}$  have far fewer free degrees than a common  $W$ .

Specifically, we synthesize each  $W$  by multiplying three low-rank matrices  $P \in \mathbb{R}^{\beta \times m}$ ,  $K \in \mathbb{R}^{\beta \times \beta}$ ,  $Q \in \mathbb{R}^{\beta \times n}$ , that is:

$$W = P^T K Q, \quad (3)$$

where  $\beta \ll \min(m, n)$  ensuring that  $P$  and  $Q$  are low-rank matrices.  $K$  can be regarded as a kernel matrix that controls the parameter size of CoLin.

##### 3.1.3. MULTI-BRANCH LINEAR PROJECTION

The low-rank design offers two primary advantages. **1) Significant parameter reduction:** For  $n$ -dimensional visual features, the projection matrix of a vanilla adapter (with intermediate dimension as half the input dimension) requires  $n^2/2$  parameters, whereas our projection matrix in Section 3.1.2 only needs  $(n+n/2)/\beta = 3n\beta/2$  parameters. Taking  $n = 768$  (common in vision models) and  $\beta = 8$ , the low-rank matrix achieves 97% parameter reduction. **2) Mitigating parameter redundancy:** As revealed in previous works (Hu et al., 2022; Karimi Mahabadi et al., 2021), the feature space of superior pre-trained models substantially exceeds the requirements of most downstream tasks. This necessitates adaptation in low-dimensional subspaces to identify optimal parameter configurations. Vanilla adapters exhibit unnecessary parameter freedom, leading to inefficient adaptation and potential overfitting in few-shot scenarios. Low-rank matrices inherently constrain this redundancy.

However, extremely low-parameter matrices may confine adapters to suboptimal subspaces, limiting overall performance. To address this without increasing inference latency, we introduce a multi-branch structure inspired by Mixture-of-Experts (MoE) (Riquelme et al., 2021) and AdaBoost (Sagi & Rokach, 2018; Thilagavathi et al., 2021) principles. Each branch  $\{P_i^T K_i Q_i\}$  captures distinct feature interpretations at its feature level, with collaborative branching enhancing adaptation robustness and decision stability. To maintain inference efficiency, we implement branch fusion through parameter summation:

$$W = \sum_{i=1}^{\alpha} W_i = \sum_{i=1}^{\alpha} P_i^T K_i Q_i. \quad (4)$$

This architecture enables: 1) Expanded solution space through branch diversity, 2) Error compensation between branches via ensemble effects, and 3) Preserved computational efficiency by linear combination. We insert CoLin into each SwinBlock twice (see Appendix E for details).

### 3.2. Complex Sharing Strategy

Compacter (Karimi Mahabadi et al., 2021) demonstrates that appropriate sharing mechanisms can enhance the efficiency and performance of adapters. To further optimize the parameter efficiency and robustness of low-rank adapters, we design two sharing mechanisms for multi-branch low-rank structures: kernel sharing and branch sharing.

#### 3.2.1. KERNEL SHARING

In adapters, the down-projection and up-projection layers correspond to feature compression and restoration, respectively. However, such compression may lead to loss of critical feature information. To preserve essential information during the feature dimension restoration process, we share the kernel matrix  $K$  of the two projection layers within each branch. We hope the sharing mechanism can promote the coherence of two projection layers during training process. Besides, the shared  $K$  also slightly reduces the number of parameters. With kernel sharing, the  $W^U$  and  $W^D$  in the proposed structure can be represented as:

$$W^U = \sum_{i=1}^{\alpha} W_i^U = \sum_{i=1}^{\alpha} (P_i^U)^T K_i Q_i^U, \quad (5)$$

$$W^D = \sum_{i=1}^{\alpha} W_i^D = \sum_{i=1}^{\alpha} (P_i^D)^T K_i Q_i^D, \quad (6)$$

where  $K_i$  is shared in  $W^U$  and  $W^D$ .

#### 3.2.2. BRANCH SHARING

Kernel sharing is performed between the up/down projections within the same branch. For different branches, we

design two distinct types of matrices. We aim for all kernel matrices to focus on branch-specific adaptations while preserving maximum flexibility. As for the higher-parameter matrices  $P$  and  $Q$ , we intend them to capture cross-task universal features or transformations, thereby enhancing the model's generalization capability.

Finally, the  $W^U$  and  $W^D$  in CoLin can be represented as:

$$W^U = \sum_{i=1}^{\alpha} W_i^U = \sum_{i=1}^{\alpha} (P^U)^T K_i Q_i^U, \quad (7)$$

$$W^D = \sum_{i=1}^{\alpha} W_i^D = \sum_{i=1}^{\alpha} (P^D)^T K_i Q_i^D, \quad (8)$$

where  $P^U$  and  $Q^U$  is shared in  $\alpha$  branches. Figure 2 presents the detailed designs of the multi-branch projection.

### 3.3. Orthogonal Optimization of the Parameter Space

The idea of low-rank synthesis can effectively reduce parameter redundancy, but it also makes the model's convergence process inefficient. To illustrate this, we first model the matrix  $W$  as a simple form  $W = PQ$ . Ideally, the change of  $W$  before and after an update can be expressed as follows:

$$\Delta W = W' - W = -\eta \nabla_W L, \quad (9)$$

where  $\eta$  denotes the learning rate and  $\nabla_W L$  is the gradient of the loss  $L$  with respect to  $W$ . In practice, when  $W = PQ$ , the parameters actually updated are  $P$  and  $Q$ . Thus,  $\Delta W$  can be approximated by the following equation (neglecting the trivial  $\eta^2$  term):

$$\begin{aligned} \Delta W &= P'Q' - PQ = (P - \eta \nabla_P L)(Q - \eta \nabla_Q L) - PQ \\ &= -\eta (\nabla_P L \cdot Q + P \cdot \nabla_Q L) + \eta^2 \cdot \nabla_P L \cdot \nabla_Q L \\ &\approx -\eta (\nabla_P L \cdot Q + P \cdot \nabla_Q L). \end{aligned} \quad (10)$$

To further analyze the above equation, we need to simplify the matrix gradients using the trace trick. First, we compute  $\nabla_Q L$ . According to the definition of loss differential, we have:

$$dL = \text{tr}(\nabla_W^T dW) = \text{tr}(\nabla_W^T \cdot P \cdot dQ), \quad (11)$$

where  $\text{tr}(\cdot)$  denotes the matrix trace. Using the cyclic permutation property of the trace  $\text{tr}(AB) = \text{tr}(BA)$ , the differential can be rewritten as  $dL = \text{tr}((P^T \nabla_W)^T \cdot dQ)$ . By the definition of matrix gradient, the derivative of  $dL$  with respect to  $dQ$  equals the transpose of the coefficient of  $dQ$  in the trace. Thus, the gradient can be expressed as:

$$\nabla_Q L = P^T \nabla_W. \quad (12)$$

Similarly,  $\nabla_P L = \nabla_W Q^T$ . Substituting these gradients into the equation for  $\Delta W$  gives:

$$\Delta W \approx -\eta \nabla_W (QQ^T + P^T P). \quad (13)$$

According to the loss differential  $dL = \text{tr}(\nabla_W^T \Delta W)$ ,  $dL$  becomes smaller when  $\Delta W$  is in the same direction as  $\nabla_W$ . In other words, the optimization efficiency of  $W$  is maximized when  $P$  and  $Q$  are orthogonal. Therefore, we expect  $P$  and  $Q$  to tend to be orthogonal, i.e., satisfying:

$$QQ^T \approx I_k \quad \text{and} \quad P^T P \approx I_k. \quad (14)$$

In this case,  $\Delta W \approx -2\eta \nabla_W$ . For detailed proof, please refer to Appendix A. To maintain the orthogonality of  $P$  and  $Q$ , we add an additional loss for each  $P_i$  and  $Q_i$ :

$$L_{PQ}^i = \|P^T P - I\|_F^2 + \|QQ^T - I\|_F^2, \quad (15)$$

where  $\|\cdot\|_F$  denotes the Frobenius Norm. Let the original loss be  $L_0$  and the proposed loss be  $L_{ort}$ , then the new loss with an extra hyper-parameter coefficient  $\lambda$  is then:

$$L = L_0 + L_{ort} = L_0 + \lambda \cdot \sum_{i=1}^n L_{PQ}^i. \quad (16)$$

### 3.4. SVD-based Initialization

From section 3.3, we know that orthogonality facilitates the convergence of adapters. To enable matrices  $P$  and  $Q$  to better maintain orthogonality, we adopt orthogonal initialization instead of the classical random initialization. Specifically, for  $P \in \mathbb{R}^{\beta \times m}$ ,  $K \in \mathbb{R}^{\beta \times \beta}$  and  $Q \in \mathbb{R}^{\beta \times n}$ , we first randomly initialize a matrix  $W_0 \in \mathbb{R}^{m \times n}$ , and then decompose  $W_0$  into  $U$ ,  $S$  and  $V$  via singular value decomposition (SVD), i.e.,

$$U, S, V = \text{SVD}(W_0). \quad (17)$$

For down-projection, we set  $P_0 = S$ ,  $K_0 = S$  and  $Q_0 = V$ . For up-projection, we only set  $P_0 = S$  and  $Q_0 = V$ . We use kaiming uniform to initialize  $W_0$ .

### 3.5. Parameter Analysis

Parameter efficiency is a metric for evaluating adapter designs. Here, we compare the number of new parameters between the standard linear layer and the proposed linear layer in the adapter. Assume that there are  $\gamma$  linear layers in the adapter, new parameters of the standard linear layer is  $\gamma mn$  (ignoring the bias), while the proposed linear layer only requires  $\gamma\beta(m + n) + \alpha\beta^2$ , which will significantly reduce the number of new parameters in the adapter.

## 4. Experiments

### 4.1. Datasets

**Object Detection.** Pascal VOC 0712 (Everingham et al., 2015) has 16k/5k training/validation images and is used for object detection tasks. We employ Swin-Large + RetinaNet for training. The evaluation metric for object detection task is the most commonly used  $AP_{box}$ .

**Semantic Segmentation.** ADE20K (Zhou et al., 2017) is a widely used semantic segmentation dataset containing 20K training and 2K validation images. We employ Swin-Large + UperNet for experiments on semantic segmentation. The evaluation metric is the most commonly used mIoU.

**Instance Segmentation.** MS COCO (Lin et al., 2014) is a representative instance segmentation dataset with 118k training images and 5k validation images. We employ Swin-Base + Cascade Mask RCNN for training. Evaluation metrics for instance segmentation task are  $AP_{box}$  and  $AP_{Mask}$ .

**Oriented Object Detection.** Oriented object detection considers angle information in the annotation and inference process, which is more challenging than horizontal object detection. Two representative remote sensing datasets, DOTA (Ding et al., 2022) and STAR (Li et al., 2025a), are selected for our experiments. We also experiment with multiple detection frameworks on the more challenging STAR dataset. The metric here is  $AP_{box}$ .

**Image Classification.** Classification tasks have been well studied in previous art. We also conduct experiments on Oxford 102 Flower (Nilsback & Zisserman, 2008), Oxford-IIIT Pet (Parkhi et al., 2012), and VOC 2007 Classification dataset (Everingham et al., 2007) to increase the broadness of our experiments. The top-1, top-5, and average accuracy of each method are reported.

### 4.2. Pre-trained Models and Toolkits

The Swin Transformer series (Liu et al., 2021) are employed as the backbone for all experiments. The pre-trained models are trained on ImageNet-22k (Deng et al., 2009), and toolkits like MMDetection (Chen et al., 2019), MM Segmentation (Contributors, 2020b), MMRotate (Zhou et al., 2022) and MMC classification (Contributors, 2020a) are used for verification. The image resolution of the pre-trained task is 224×224. Most tasks employ Swin-Large as the backbone. Backbones for COCO, DOTA, and STAR are Swin-Base, considering the memory consumption of these tasks.

### 4.3. Baselines

We compare CoLin with multiple recent methods. Baselines can be grouped into methods without or with extra structure.

**Without extra structure.** FULL: Update all parameters in

**Table 1. Results of baselines and our method on Pascal VOC and ADE20K benchmarks.** Swin-L is employed as the pre-trained model here. We present the numbers and percentages of trainable backbone parameters on the left and all the performances on the right. \* denotes the trainable parameters in backbones. The best AP/mIoU in each column is bolded.

Swin-L (198M)	Trained* Params	%	$\Delta_{Full}$	Extra Structure	Pascal VOC (RetinaNet)		ADE20K (UperNet)	
					AP <sub>Box</sub>	$\Delta_{Full}$	mIoU	$\Delta_{Full}$
<b>Baselines</b>								
FULL	198.58 M	100.00 %	-	✗	83.70 %	-	51.18 %	-
FIXED	0.00 M	0.00 %	- 100.00 %	✗	83.80 %	+ 0.10 %	46.84 %	- 4.34 %
BITFIT	0.30 M	0.15 %	- 99.85 %	✗	85.40 %	+ 1.70 %	48.37 %	- 2.81 %
NORMTUNING	0.10 M	0.05 %	- 99.95 %	✗	85.50 %	+ 1.80 %	47.89 %	- 3.29 %
PARTIAL-1	28.77 M	14.53 %	- 85.47 %	✗	85.50 %	+ 1.80 %	47.44 %	- 3.74 %
ADAPTER	4.61 M	2.33 %	- 97.67 %	✓	86.70 %	+ 3.00 %	50.78 %	- 0.40 %
LORA	4.57 M	2.31 %	- 97.69 %	✓	85.40 %	+ 1.70 %	50.34 %	- 0.84 %
ADAPTFORMER	2.34 M	1.18 %	- 98.82 %	✓	86.60 %	+ 2.90 %	50.83 %	- 0.35 %
LORAND	5.20 M	2.62 %	- 97.38 %	✓	86.90 %	+ 3.20 %	50.93 %	- 0.25 %
<b>Our Method</b>								
<b>CoLin</b>	2.39 M	1.23 %	-98.77 %	✓	<b>87.50 %</b>	<b>+ 3.80 %</b>	<b>51.28 %</b>	<b>+0.10 %</b>

**Table 2. Results of baselines and our method on COCO benchmarks.** Swin-B is employed as the pre-trained model here. We present the numbers and percentages of trainable backbone parameters on the left and all the performances on the right. \* denotes the trainable parameters in backbones. The best AP in each column is bolded.

Swin-B (89M)	Trained* Params	%	$\Delta_{Full}$	Extra Structure	COCO (Cascade Mask R-CNN)			
					AP <sub>Box</sub>	$\Delta_{Full}$	AP <sub>Mask</sub>	$\Delta_{Full}$
<b>Baselines</b>								
FULL	89.14 M	100.00 %	-	✗	52.40 %	-	45.10 %	-
FIXED	0.00 M	0.00 %	- 100.00 %	✗	48.00 %	- 4.40 %	41.60 %	- 3.50 %
BITFIT	0.21 M	0.23 %	- 99.77 %	✗	50.10 %	- 2.30 %	43.60 %	- 1.50 %
NORMTUNING	0.06 M	0.07 %	- 99.93 %	✗	50.10 %	- 2.30 %	43.50 %	- 1.60 %
PARTIAL-1	12.95 M	14.53 %	- 85.47 %	✗	50.60 %	- 1.80 %	43.70 %	- 1.40 %
ADAPTER	3.19 M	3.58 %	- 96.42 %	✓	52.10 %	- 0.30 %	45.00 %	- 0.10 %
LORA	3.06 M	3.43 %	- 96.57 %	✓	50.40 %	- 2.00 %	43.90 %	- 1.20 %
ADAPTFORMER	1.60 M	1.79 %	- 98.21 %	✓	51.70 %	- 0.70 %	44.60 %	- 0.50 %
LORAND	4.68 M	5.23 %	- 94.77 %	✓	51.90 %	- 0.50 %	44.70 %	- 0.40 %
<b>Our Method</b>								
<b>CoLin</b>	1.71 M	1.97 %	-98.03 %	✓	<b>52.90 %</b>	<b>+ 0.50 %</b>	<b>45.50 %</b>	<b>+ 0.40 %</b>

the framework. FIXED: Fix the backbone and update other parameters. BITFIT (Ben Zaken et al., 2022): Update bias in backbone and parameters outside of backbone. NORMTUNING (Giannou et al., 2023): Update norm layers in backbone and parameters outside the backbone. PARTIAL-1 (Yosinski et al., 2014): Update the last block in the backbone and parameters outside the backbone.

**With extra structure.** ADAPTER (Houlsby et al., 2019): Add standard adapter layers after the MSA/MLP layers of each SwinBlock. LORA (Hu et al., 2022): Add parallel learnable matrices to multi-head attention weights. ADAPTFORMER (Chen et al., 2022): Add parallel adapter layers with scale weights to each MLP layer. LORAND (Yin et al., 2023): Add LoRand++ ( $\alpha=4, \beta=16$ ) layers after the MSA/MLP of each SwinBlock. LoRand++ has the best performance among its variants, so the most challenging

setting is chosen for comparison. MONA (Yin et al., 2025a): Add Mona in the same way as the ADAPTER (Table 5).

#### 4.4. Main Results

Table 1 reports the performance of CoLin on object detection (Pascal VOC) and semantic segmentation (ADE20k) tasks. The results demonstrate that CoLin outperforms full fine-tuning and other representative methods while fine-tuning only 1.23% of the backbone parameters. Notably, all PEFT methods surpass full fine-tuning on the relatively simple Pascal VOC dataset, serving as a low-resource setting in this context. This finding is consistent with results from the NLP domain (cite), corroborating that PEFT methods exhibit distinct advantages for few-shot learning tasks. Table 2 extends the evaluation to CoLin’s performance on fine-grained instance segmentation using the COCO dataset.

Table 3. Results of baselines and our method on three classification datasets. Swin-L is employed as the pre-trained model here. We present top-1 accuracy (%) and top-5 accuracy (%) of each dataset. The best result in each column is bolded.

Method	Flowers102		OxfordPets		VOC2007		Average	
	top-1 acc.	top-5 acc.						
<b>Baselines</b>								
FULL	99.5772	99.8536	94.6579	99.6257	84.1276	96.9507	92.7876	98.8100
FIXED	99.3007	99.8374	94.2219	99.9182	85.0162	98.9499	92.8463	99.5685
BITFIT	99.5772	99.8211	95.3393	99.9182	85.6018	99.3336	93.5061	99.6910
NORMTUNING	99.5284	99.8374	95.2303	99.8910	85.5210	99.2528	93.4266	99.6604
PARTIAL-1	99.6585	99.8374	95.3938	99.8637	84.9354	98.6066	93.3292	99.4359
ADAPTER	99.5934	99.8536	95.3393	99.8092	87.0355	99.1317	93.9894	99.6144
LORA	99.5446	99.8536	95.1485	99.8910	85.7028	99.3134	93.4653	99.6860
ADAPTFORMER	99.5609	99.8536	95.2576	99.8365	86.2884	99.2730	93.7023	99.6544
LoRAND	99.5725	99.8536	95.3515	99.8910	86.6534	99.3741	93.8591	99.7062
<b>Our Method</b>								
<b>CoLin</b>	<b>99.6619</b>	<b>99.8816</b>	<b>95.4336</b>	<b>99.9182</b>	<b>87.1132</b>	<b>99.6108</b>	<b>94.0696</b>	<b>99.8035</b>

Table 4. Results on DOTA and STAR benchmarks. Swin-B is employed as the pre-trained model here. The best AP in each column is bolded.

Swin-B (89M)	Oriented R-CNN (Faster R-CNN)		KLD (RetinaNet)	H2RBox-v2 (FCOS)
	DOTA-v1.0	STAR	STAR	STAR
<b>Baselines</b>				
FULL	78.31 %	38.63 %	30.33 %	30.29 %
FIXED	74.10 %	30.83 %	23.81 %	26.01 %
BITFIT	76.05 %	34.51 %	28.17 %	29.41 %
NORMTUNING	75.82 %	33.13 %	27.12 %	27.79 %
PARTIAL-1	75.72 %	33.96 %	28.53 %	28.89 %
ADAPTER	78.27 %	37.97 %	30.35 %	30.24 %
LoRA	75.91 %	33.80 %	27.48 %	28.95 %
ADAPTFORMER	77.43 %	35.95 %	29.36 %	30.11 %
LoRAND	77.65 %	36.44 %	29.83 %	28.85 %
<b>Our Method</b>				
<b>CoLin</b>	<b>78.39 %</b>	<b>39.22 %</b>	<b>30.68 %</b>	<b>31.14%</b>

Similarly, CoLin achieves superior performance to full fine-tuning and competing approaches by fine-tuning only 1.97% of new parameters. Given that instance segmentation imposes more stringent demands on model architectures than object detection and standard semantic segmentation, the results in Table 2 more robustly demonstrate CoLin’s efficacy on complex vision tasks. As image classification tasks receive considerable attention in the research community, we present the performance of all methods across three widely used classification datasets in Table 3. The results indicate that CoLin also delivers promising performance in image classification. Notably, due to the narrow performance gaps among these methods on classification datasets, our focus is directed toward their performance differences on complex tasks. Lastly, Table 4 evaluates the performance of all methods on the remote sensing rotated object detection task. Since pre-trained models are initialized on natural-scene data, these results also characterize the cross-domain

Table 5. Comparisons with Mona. CoLin outperforms Mona on param flexibility and inference speed (tested on 8 × RTX 4090).

Module	Task/Backbone	% <sub>Full</sub>	Per.	Inference Speed
MONA	COCO/Swin-B	4.67%	53.4%	40.1 tasks/s
COLIN (D128K64)	COCO/Swin-B	4.59%	53.3%	46.3 tasks/s
COLIN (D100K28)	COCO/Swin-B	1.97%	52.9%	47.5 tasks/s
MONA	VOC/Swin-L	2.56%	87.3%	61.9 tasks/s
COLIN (D128K64)	VOC/Swin-L	2.52%	87.3%	73.8 tasks/s
COLIN (D100K28)	VOC/Swin-L	1.23%	87.5%	75.1 tasks/s

transfer capabilities of the evaluated methods. Specifically, results in Table 4 demonstrate that CoLin maintains its superiority over full fine-tuning and representative baselines in cross-domain transfer scenarios.

Beyond the above methods, we conduct a multi-dimensional comparison between CoLin and Mona (Yin et al., 2025a). For a more intuitive comparison, Table 5 presents the parameter count, performance, and inference speed of two variants of CoLin against Mona under different settings. When parameter are comparable, CoLin achieves performance on par with Mona. CoLin’s advantages over Mona are twofold: 1) CoLin can flexibly adjust the number of new parameters, thereby regulating the parameter redundancy of the adapter. Results on Pascal VOC demonstrate that fewer parameters yield superior performance in few-shot scenarios. 2) CoLin exhibits lower inference latency than Mona. Specifically, Mona incorporates multiple DWConv layers, one pointwise conv, and two linear projections, whereas CoLin only involves one DWConv layer and two linear projections during inference. Notably, the multi-branch structure of CoLin employed in training phase can be converted into standard linear layers during inference. Overall, **CoLin boosts inference speed by nearly 20% than Mona** while still achieving impressive performance, which significantly lowers the per-inference cost for commercial enterprises.

In addition to the comparative experiments, we design a sim-

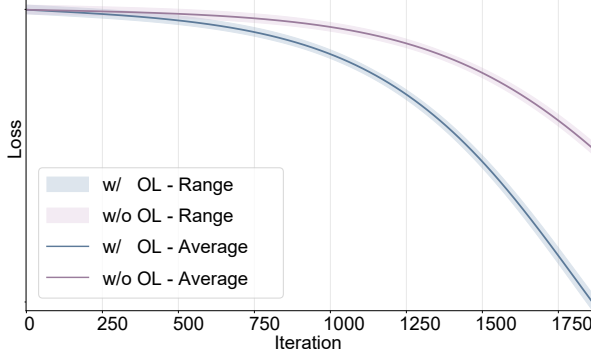


**Figure 3. Convergence simulation.** Theoretical analysis and simulation experiments demonstrate that in low-rank synthesis scenarios, orthogonality (blue) significantly enhances the overall convergence efficiency of the model.

ulation experiments to illustrate the role of orthogonal loss in the convergence process of low-rank composite matrices. Specifically, we devise a simple loss function to drive two groups of matrices to approximate a randomly generated target matrix  $W \in \mathbb{R}^{m \times n}$  via gradient descent. For matrices  $P \in \mathbb{R}^{k \times m}$  and  $Q \in \mathbb{R}^{k \times n}$ , we minimize the loss function  $\text{Loss} = \|W - P^\top Q\|_2$  to make  $P^\top Q$  approach  $W$ . We set the hyperparameters as  $[m, k, n] = [100, 30, 5000]$  and the learning rate (lr) to  $10^{-5}$ , then calculate the mean and range of the loss values over 20 random seeds. Figure 3 depicts the loss variations of the two matrix groups during convergence, where the blue curve corresponds to the setup with the additional orthogonal loss (OL) and the purple curve denotes the setup without OL. As can be observed, the convergence efficiency of the blue group is significantly higher than that of the purple group at the same number of iterations. Section 3.3 and Figure 3 clarify the convergence issues of low-rank composite matrices from both theoretical and experimental perspectives, which effectively explains the superior performance of CoLin. Appendix B provides simulation results on more matrix sizes. Additionally, we discuss limitations and future directions in Appendix C.

#### 4.5. Ablations

**Internal Design.** Table 6 presents the ablation results of CoLin during the optimization process. Vanilla version denotes the multi-branch low-rank adapter architecture with a sharing mechanism (as illustrated in Figure 2). OL refers to the orthogonal loss introduced in Section 3.3, while SVDinit denotes the initialization method described in Section 3.4. Without matrix optimization, CoLin achieves performance comparable to full fine-tuning by tuning only about 1% of the total parameters (see Tables 2 and 1), but fails to outperform it. The incorporation of orthogonal loss enables CoLin to surpass full fine-tuning on both few-shot and complex tasks. The SVD initialization method facilitates the low-rank matrices to converge toward orthogonality, which

**Table 6. Design ablations.** Multiple necessary components enable CoLin to outperform full fine-tuning with 1% new parameters.

Method	Pascal VOC	COCO
VALLINA	87.0 %	52.0 %
+OL	87.3 %	52.6 %
+OL+SVDINIT	87.5 %	52.9 %

further enhances the convergence efficiency of the orthogonal loss. Table 6 demonstrate that the optimization designs proposed in this work can effectively boost the performance of visual adapters, which experimentally validates the theoretical analysis presented in Section 3.3.

**Table 7. Ablations on hyperparameters.** Results under different value of  $D$ ,  $K$ , and  $B$ .

Param	Value	% Full	Per. On VOC
$D$	128	1.27%	87.5%
	100	1.23%	87.5%
	72	1.18%	87.2%
$K$	32	1.40%	87.6%
	28	1.23%	87.5%
	16	0.72%	86.9%
$B$	8	1.23%	87.5%
	4	1.23%	87.5%
	1	1.23%	87.2%

**Hyperparameter.** We conduct ablation studies on three key hyperparameters.  $D$  denotes the projection dimension,  $K$  denotes the kernel size, and  $B$  denotes the number of branches. For all experiments, the baseline configuration is set as  $[D, K, B] = [100, 28, 4]$ , where only one of the three hyperparameters is varied in each individual trial. Results in Table 7 show that kernel size ( $K$ ) exerts the most significant impact on the number of trainable parameters. By contrast, adjustments to  $D$  and  $B$  yield negligible effects on the trainable parameter count, owing to the sharing mechanism. Considering the trade-off between parameter count and model performance, we ultimately adopt  $[D, K, B] = [100, 28, 4]$  as the standard configuration for CoLin.

## 5. Conclusion

We propose CoLin, which surpasses full fine-tuning with only about 1% backbone params on visual recognition tasks for the first time. With matrix theory, we analyze and optimize the gradient backpropagation process of the low-rank composite matrices, effectively enhancing CoLin’s transfer efficiency of visual features. Extensive experiments demonstrate that the proposed method outperforms full fine-tuning across a broad range of visual recognition tasks. As large vision models continue to expand in parameter and knowledge capacity, the transfer potential of CoLin is poised to be further amplified for both scholars and developers.

## Impact Statement

This paper presents work whose goal is to advance the field of Machine Learning. There are many potential societal consequences of our work, none which we feel must be specifically highlighted here.

## References

Awais, M., Naseer, M., Khan, S., Anwer, R. M., Cholakkal, H., Shah, M., Yang, M.-H., and Khan, F. S. Foundation models defining a new era in vision: A survey and outlook. *IEEE TPAMI*, 47(4):2245–2264, 2025.

Ben Zaken, E., Goldberg, Y., and Ravfogel, S. BitFit: Simple parameter-efficient fine-tuning for transformer-based masked language-models. In *Proceedings of the Association for Computational Linguistics*, pp. 1–9, 2022.

Chen, K., Wang, J., Pang, J., Cao, Y., Xiong, Y., Li, X., Sun, S., Feng, W., Liu, Z., Xu, J., et al. Mmdetection: Open mmlab detection toolbox and benchmark. *arXiv preprint arXiv:1906.07155*, 2019.

Chen, S., GE, C., Tong, Z., Wang, J., Song, Y., Wang, J., and Luo, P. Adaptformer: Adapting vision transformers for scalable visual recognition. In *NeurIPS*, volume 35, pp. 16664–16678, 2022.

Contributors, M. Openmmlab’s image classification toolbox and benchmark. <https://github.com/open-mmlab/mmclassification>, 2020a.

Contributors, M. MMSegmentation: Openmmlab semantic segmentation toolbox and benchmark. <https://github.com/open-mmlab/mmsegmentation>, 2020b.

Deng, J., Dong, W., Socher, R., Li, L.-J., Li, K., and Fei-Fei, L. Imagenet: A large-scale hierarchical image database. In *CVPR*, pp. 248–255, 2009.

Ding, J., Xue, N., Xia, G.-S., Bai, X., Yang, W., Yang, M. Y., Belongie, S., Luo, J., Datcu, M., Pelillo, M., and Zhang, L. Object detection in aerial images: A large-scale benchmark and challenges. *IEEE TPAMI*, 44(11):7778–7796, 2022.

Ding, N., Qin, Y., Yang, G., Wei, F., Yang, Z., Su, Y., Hu, S., Chen, Y., Chan, C.-M., Chen, W., et al. Parameter-efficient fine-tuning of large-scale pre-trained language models. *Nature machine intelligence*, 5(3):220–235, 2023.

Du, Y., Liu, Z., Li, J., and Zhao, W. X. A survey of vision-language pre-trained models. *arXiv preprint arXiv:2202.10936*, 2022.

Dutt, R., Ericsson, L., Sanchez, P., Tsaftaris, S., and Hospedales, T. Parameter-efficient fine-tuning for medical image analysis: The missed opportunity. In *Proceedings of Medical Imaging with Deep Learning*, pp. 1–20, 2024.

Everingham, M., Van Gool, L., Williams, C. K. I., Winn, J., and Zisserman, A. The PASCAL Visual Object Classes Challenge 2007 (VOC2007) Results. <http://www.pascal-network.org/challenges/VOC/voc2007/workshop/index.html>, 2007.

Everingham, M., Eslami, S. A., Van Gool, L., Williams, C. K., Winn, J., and Zisserman, A. The pascal visual object classes challenge: A retrospective. *IJCV*, 111(1):98–136, 2015.

Franklin, J. N. *Matrix theory*. Courier Corporation, 2000.

Gao, H., Wang, Z., Li, Y., Long, K., Yang, M., and Shen, Y. A survey for foundation models in autonomous driving. In *International Conference on Computer Vision and Data Mining*, pp. 63–71, 2025.

Giannou, A., Rajput, S., and Papailiopoulos, D. The expressive power of tuning only the norm layers. *arXiv preprint arXiv:2302.07937*, 2023.

Han, Z., Gao, C., Liu, J., Zhang, J., and Zhang, S. Q. Parameter-efficient fine-tuning for large models: A comprehensive survey. *Transactions on Machine Learning Research*, 2024.

He, K., Zhang, X., Ren, S., and Sun, J. Deep residual learning for image recognition. In *CVPR*, pp. 770–778, 2016.

Houlsby, N., Giurgiu, A., Jastrzebski, S., Morrone, B., De Laroussilhe, Q., Gesmundo, A., Attariyan, M., and Gelly, S. Parameter-efficient transfer learning for NLP. In *ICML*, volume 97, pp. 2790–2799, 2019.

Hu, E. J., yelong shen, Wallis, P., Allen-Zhu, Z., Li, Y., Wang, S., Wang, L., and Chen, W. LoRA: Low-rank adaptation of large language models. In *ICLR*, 2022.

Hu, L., Lu, W., Yu, H., Yin, D., Sun, X., and Fu, K. Tea: A training-efficient adapting framework for tuning foundation models in remote sensing. *IEEE Transactions on Geoscience and Remote Sensing*, 62:1–18, 2024a.

Hu, L., Yu, H., Lu, W., Yin, D., Sun, X., and Fu, K. Airs: Adapter in remote sensing for parameter-efficient transfer learning. *IEEE Transactions on Geoscience and Remote Sensing*, 62:1–18, 2024b.

Jia, M., Tang, L., Chen, B.-C., Cardie, C., Belongie, S., Hariharan, B., and Lim, S.-N. Visual prompt tuning. In *ECCV*, pp. 709–727. Springer, 2022.

Karimi Mahabadi, R., Henderson, J., and Ruder, S. Comacter: Efficient low-rank hypercomplex adapter layers. In *NeurIPS*, volume 34, pp. 1022–1035, 2021.

Li, Y., Wang, L., Wang, T., Yang, X., Luo, J., Wang, Q., Deng, Y., Wang, W., Sun, X., Li, H., Dang, B., Zhang, Y., Yu, Y., and Yan, J. Star: A first-ever dataset and a large-scale benchmark for scene graph generation in large-size satellite imagery. *IEEE TPAMI*, 47(3):1832–1849, 2025a.

Li, Z., Wu, X., Du, H., Nghiem, H., and Shi, G. Benchmark evaluations, applications, and challenges of large vision language models: A survey. *arXiv preprint arXiv:2501.02189*, 1, 2025b.

Liang, J., Huang, W., Wan, G., Yang, Q., and Ye, M. LoraSculpt: Sculpting lora for harmonizing general and specialized knowledge in multimodal large language models. In *CVPR*, pp. 26170–26180, 2025.

Lin, T.-Y., Maire, M., Belongie, S., Hays, J., Perona, P., Ramanan, D., Dollár, P., and Zitnick, C. L. Microsoft coco: Common objects in context. In *ECCV*, pp. 740–755. Springer, 2014.

Liu, S.-Y., Wang, C.-Y., Yin, H., Molchanov, P., Wang, Y.-C. F., Cheng, K.-T., and Chen, M.-H. DoRA: Weight-decomposed low-rank adaptation. In *ICML*, volume 235, pp. 32100–32121, 2024.

Liu, Y.-C., MA, C.-Y., Tian, J., He, Z., and Kira, Z. Polyhisto: Parameter-efficient multi-task adaptation for dense vision tasks. In *NeurIPS*, volume 35, pp. 36889–36901, 2022.

Liu, Z., Lin, Y., Cao, Y., Hu, H., Wei, Y., Zhang, Z., Lin, S., and Guo, B. Swin transformer: Hierarchical vision transformer using shifted windows. In *ICCV*, pp. 9992–10002, 2021.

Nilsback, M.-E. and Zisserman, A. Automated flower classification over a large number of classes. In *Indian Conference on Computer Vision, Graphics & Image Processing*, pp. 722–729, 2008.

Pan, J., Lin, Z., Zhu, X., Shao, J., and Li, H. St-adapter: Parameter-efficient image-to-video transfer learning. In *NeurIPS*, volume 35, pp. 26462–26477, 2022.

Parkhi, O. M., Vedaldi, A., Zisserman, A., and Jawahar, C. V. Cats and dogs. In *CVPR*, pp. 3498–3505, 2012.

Riquelme, C., Puigcerver, J., Mustafa, B., Neumann, M., Jenatton, R., Susano Pinto, A., Keysers, D., and Houlsby, N. Scaling vision with sparse mixture of experts. In *NeurIPS*, volume 34, pp. 8583–8595, 2021.

Rücklé, A., Geigle, G., Glockner, M., Beck, T., Pfeiffer, J., Reimers, N., and Gurevych, I. AdapterDrop: On the efficiency of adapters in transformers. In *Proceedings of the Conference on Empirical Methods in Natural Language Processing*, pp. 7930–7946, 2021.

Sagi, O. and Rokach, L. Ensemble learning: A survey. *WIREs Data Mining and Knowledge Discovery*, 8(4):e1249, 2018.

Thilagavathi, B., Suthendran, K., and Srujanraju, K. Evaluating the adaboost algorithm for biometric-based face recognition. In *Data Engineering and Communication Technology*, pp. 669–678, 2021.

Xia, J., Zhang, C., Zhang, Y., Zhou, C., Wang, Z., Liu, B., and Yin, D. Dape: Dual-stage parameter-efficient fine-tuning for consistent video editing with diffusion models. *arXiv preprint arXiv:2505.07057*, 2025.

Yin, D., Yang, Y., Wang, Z., Yu, H., Wei, K., and Sun, X. 1% vs 100%: Parameter-efficient low rank adapter for dense predictions. In *CVPR*, pp. 20116–20126, 2023.

Yin, D., Han, X., Li, B., Feng, H., and Bai, J. Parameter-efficient is not sufficient: Exploring parameter, memory, and time efficient adapter tuning for dense predictions. In *ACM Multimedia*, pp. 1398–1406, 2024.

Yin, D., Hu, L., Li, B., Zhang, Y., and Yang, X. 5% > 100%: Breaking performance shackles of full fine-tuning on visual recognition tasks. In *CVPR*, pp. 20071–20081, 2025a.

Yin, D., Zhao, T.-F., Fan, D.-P., Li, S., Du, B., Sun, X., and Hu, S.-M. Remote sensing tuning: A survey. *Computational Visual Media*, 11(5):897–937, 2025b.

Yosinski, J., Clune, J., Bengio, Y., and Lipson, H. How transferable are features in deep neural networks? In *NeurIPS*, volume 2, pp. 3320–3328, 2014.

Yu, B. X., Chang, J., Wang, H., Liu, L., Wang, S., Wang, Z., Lin, J., Xie, L., Li, H., Lin, Z., Tian, Q., and Chen, C. W. Visual tuning. *ACM Comput. Surv.*, 56(12), 2024.

Zhou, B., Zhao, H., Puig, X., Fidler, S., Barriuso, A., and Torralba, A. Scene parsing through ade20k dataset. In *CVPR*, pp. 5122–5130, 2017.

Zhou, Y., Yang, X., Zhang, G., Wang, J., Liu, Y., Hou, L., Jiang, X., Liu, X., Yan, J., Lyu, C., Zhang, W., and Chen, K. Mmrotate: A rotated object detection benchmark using pytorch. In *ACM Multimedia*, pp. 7331–7334, 2022.

Table 8. Definitions of core symbols.

Symbol	Description
$W$	Projection matrix in the adapter (dimension $m \times n$ ), with the goal of minimizing the loss $L$ by optimizing $W$
$P, Q$	Low-rank decomposition factors: $P \in \mathbb{R}^{\beta \times m}, Q \in \mathbb{R}^{\beta \times n}$ , satisfying $W = PQ$
$L(W)$	Task loss function (scalar), dependent on the projection matrix $W$
$\nabla_W L$	Gradient of the loss $L$ with respect to $W$ (dimension $m \times n$ )
$\eta$	Learning rate (positive number, typically in the range $10^{-5} \sim 10^{-3}$ , satisfying $\eta^2 \ll \eta$ )
$\text{tr}(\cdot)$	Matrix trace (sum of diagonal elements)
$\ \cdot\ _F$	Frobenius norm (square root of the sum of squares of all matrix elements)
$I_k$	$k$ -dimensional identity matrix (here $k = \beta$ , i.e., the rank of the low-rank decomposition)

## A. Detailed proof of Section 3.3

### A1. Assumptions and Notation Definitions

To rigorously complete the proof, we first clarify the definitions of core symbols and basic assumptions in this section:

**Basic Assumptions:**

1. The matrix differential satisfies the product rule: For any differentiable matrices  $A, B$ ,  $d(AB) = AdB + dAB$ ;
2. The learning rate  $\eta$  is sufficiently small, and the higher-order infinitesimal term  $\eta^2$  can be neglected;
3. The loss function  $L(W)$  is twice differentiable with respect to  $W$ , and the gradient  $\nabla_W L$  exists and is continuous.

### A2. Update Rule of $W$ in the Ideal Case

The core idea of gradient descent is to update parameters along the negative gradient direction of the loss function to minimize the loss. For the projection matrix  $W$ , the ideal update rule is:

$$W' = W - \eta \nabla_W L$$

, where  $W'$  denotes the updated matrix. Defining the parameter update amount  $\Delta W = W' - W$ , we have in the ideal case:

$$\Delta W = -\eta \nabla_W L. \quad (\text{A1})$$

At this point, the differential of the loss is  $dL = \text{tr}(\nabla_W^T \Delta W) = -\eta \text{tr}(\nabla_W^T \nabla_W)$ . Since  $\text{tr}(\nabla_W^T \nabla_W) = \|\nabla_W\|_F^2 \geq 0$ , the loss can decrease with maximum efficiency.

### A3. Derivation of the Actual $\Delta W$ Under Low-Rank Decomposition

When  $W = PQ$ , the actual objects of parameter update are the low-rank factors  $P$  and  $Q$ , rather than  $W$  itself. Assume the update rules for  $P$  and  $Q$  are:

$$P' = P - \eta \nabla_P L, \quad Q' = Q - \eta \nabla_Q L, \quad (\text{A2})$$

where  $\nabla_P L$  and  $\nabla_Q L$  are the gradients of the loss  $L$  with respect to  $P$  and  $Q$ , respectively.

#### A3.1 EXPANSION OF $\Delta W$

The updated  $W' = P'Q'$ , thus:

$$\begin{aligned} \Delta W &= W' - W = (P - \eta \nabla_P L)(Q - \eta \nabla_Q L) - PQ \\ &= PQ - \eta \nabla_P L \cdot Q - \eta P \cdot \nabla_Q L + \eta^2 \nabla_P L \cdot \nabla_Q L - PQ \\ &= -\eta (\nabla_P L \cdot Q + P \cdot \nabla_Q L) + \eta^2 \nabla_P L \cdot \nabla_Q L. \end{aligned}$$

Since the learning rate  $\eta \ll 1$ , the contribution of the higher-order term  $\eta^2 \nabla_P L \cdot \nabla_Q L$  to  $\Delta W$  is negligible. Therefore:

$$\Delta W \approx -\eta (\nabla_P L \cdot Q + P \cdot \nabla_Q L). \quad (\text{A3})$$

#### A3.2 DERIVATION OF GRADIENTS $\nabla_P L$ AND $\nabla_Q L$

To solve  $\nabla_P L$  and  $\nabla_Q L$ , we need to use the *trace trick* for matrix derivatives, which relies on two key properties of the trace operation:

1. Cyclic permutation property: For any compatible matrices  $A, B$ ,  $\text{tr}(AB) = \text{tr}(BA)$ ;
2. Linearity: For any matrices  $A, B$  and constant  $c$ ,  $\text{tr}(A + B) = \text{tr}(A) + \text{tr}(B)$  and  $\text{tr}(cA) = c\text{tr}(A)$ .

**Step 1: Definition of Loss Differential** For the loss function  $L(W)$ , its differential can be expressed as the inner product of the gradient and the parameter differential, in matrix form:

$$dL = \text{tr}(\nabla_W^T dW), \quad (\text{A4})$$

where  $dW$  is the differential matrix of  $W$ .

**Step 2: Substitute the Low-Rank Decomposition**  $W = PQ$  According to the product rule of matrix differentials,  $dW = PdQ + dPQ$  (where  $dP$  and  $dQ$  are the differential matrices of  $P$  and  $Q$ , respectively). Substituting this into Equation (A4):

$$dL = \text{tr}(\nabla_W^T (PdQ + dPQ)) = \text{tr}(\nabla_W^T PdQ) + \text{tr}(\nabla_W^T dPQ).$$

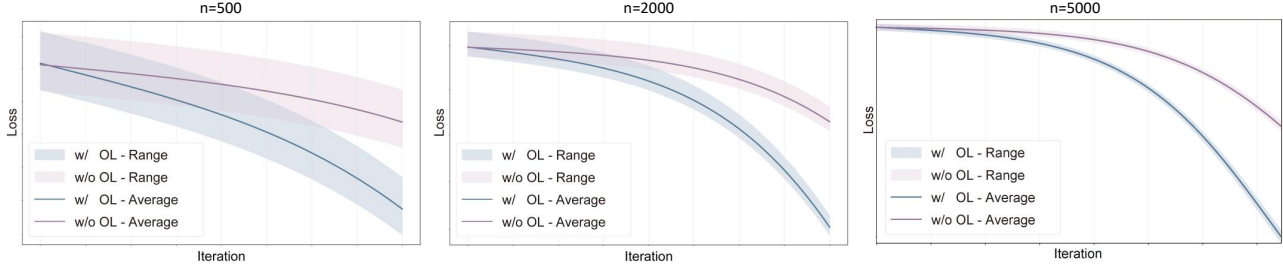


Figure 4. Impact of Orthogonal Loss on Matrices of Different Sizes. All iterations range from 0 to 2000. The difference among the three figures lies in the second dimension size of the matrices. As the size increases, the benefit of adding orthogonal loss becomes greater.

### Step 3: Differentiate with Respect to $dQ$ (Derive $\nabla_Q L$ )

Applying the cyclic permutation property of the trace to the first term above:

$$\text{tr}(\nabla_W^T P dQ) = \text{tr}((P^T \nabla_W)^T dQ).$$

By the definition of matrix gradient: If  $dL = \text{tr}(G^T dX)$ , then  $\nabla_X L = G$ . Here,  $X = Q$ , so:

$$\nabla_Q L = P^T \nabla_W. \quad (\text{A5})$$

### Step 4: Differentiate with Respect to $dP$ (Derive $\nabla_P L$ )

Applying the cyclic permutation property of the trace to the second term above:

$$\text{tr}(\nabla_W^T dP Q) = \text{tr}(Q \nabla_W^T dP) = \text{tr}((\nabla_W Q^T)^T dP).$$

Similarly, by the definition of matrix gradient,  $X = P$ , so:

$$\nabla_P L = \nabla_W Q^T. \quad (\text{A6})$$

### A3.3 SIMPLIFICATION OF $\Delta W$ AFTER SUBSTITUTING GRADIENTS

Substituting Equations (A5) and (A6) into Equation (A3):

$$\begin{aligned} \Delta W &\approx -\eta ((\nabla_W Q^T) \cdot Q + P \cdot (P^T \nabla_W)) \\ &= -\eta (\nabla_W (Q Q^T) + (P^T P) \nabla_W). \end{aligned} \quad (\text{A7})$$

Due to the associativity of matrix multiplication,  $\nabla_W (Q Q^T) = \nabla_W \cdot Q Q^T$  (where  $Q Q^T$  is a  $\beta \times \beta$  matrix, compatible with the left multiplication of  $\nabla_W$ ), and  $(P^T P) \nabla_W = P^T P \cdot \nabla_W$ . Thus, the common factor  $\nabla_W$  can be factored out:

$$\Delta W \approx -\eta \nabla_W (Q Q^T + P^T P). \quad (\text{A8})$$

## A4. Impact of Orthogonality on Optimization Efficiency

### A4.1 CORE CRITERION FOR OPTIMIZATION EFFICIENCY

The efficiency of loss reduction is determined by  $dL = \text{tr}(\nabla_W^T \Delta W)$ : When  $\Delta W$  is aligned with  $-\nabla_W$ ,  $dL$  reaches

its minimum (the loss decreases the fastest). Combining Equation (A8):

$$dL \approx -\eta \text{tr}(\nabla_W^T \nabla_W (Q Q^T + P^T P)).$$

If  $Q Q^T + P^T P = c I_\beta$  (where  $c > 0$  is a constant), then:

$$dL \approx -\eta c \text{tr}(\nabla_W^T \nabla_W).$$

At this point,  $\Delta W$  is completely aligned with  $-\nabla_W$ , and the optimization efficiency is maximized (the constant  $c$  only affects the step size, which can be adjusted via the learning rate  $\eta$ ).

### A4.2 OPTIMALITY OF ORTHOGONALITY

When  $P$  and  $Q$  satisfy the *orthogonality condition*:

$$P^T P \approx I_\beta, \quad Q Q^T \approx I_\beta, \quad (\text{A10})$$

we have  $Q Q^T + P^T P \approx I_\beta + I_\beta = 2 I_\beta$ . Substituting into Equation (A8):

$$\Delta W \approx -2\eta \nabla_W. \quad (\text{A11})$$

At this point,  $\Delta W$  is completely consistent with the ideal update direction (Equation (A1)) (only the step size coefficient is 2, which does not affect the direction), and the loss reduction efficiency is maximized.

Conversely, if  $P$  or  $Q$  is non-orthogonal (e.g.,  $P^T P = 3 I_\beta$ ,  $Q Q^T = 0.5 I_\beta$ ), then  $Q Q^T + P^T P = 3.5 I_\beta$ , leading to  $\Delta W \approx -3.5\eta \nabla_W$ , where the step size deviates from the optimal value. More critically, if  $Q Q^T + P^T P$  is a non-diagonal matrix, the direction of  $\Delta W$  will deviate from  $-\nabla_W$ , significantly reducing optimization efficiency and even causing training oscillations.

## A6. Conclusion

The detailed proof above demonstrates that the low-rank decomposition  $W = P Q$  causes the parameter update direction to deviate from the ideal negative gradient direction. The orthogonality of  $P$  and  $Q$  is the key to solving this problem—orthogonality enables  $\Delta W$  to approximate the ideal update direction, maximizing optimization efficiency.

By introducing the orthogonal regularization loss, this orthogonality can be maintained during training, ultimately improving the convergence speed and performance of the low-rank adapter.

## B. The Impact of Orthogonality on Matrices of Different Sizes

Figure 3 illustrates the convergence processes under the setting of  $[m, k, n] = [100, 30, 5000]$ . To further investigate the impact of orthogonal loss on matrices of different sizes, we conduct experiments across a broader range of size configurations. From left to right, Figure 4 presents the convergence processes corresponding to matrix sizes  $n = [500, 2000, 5000]$ . All three sets of results are obtained from experiments with 20 random seeds. It can be observed that orthogonality yields a more pronounced improvement in convergence for larger matrices. Low-rank synthesis is prevalent in the era of large models (e.g., LoRA, LoRand, CoLin). As the dimensionality of large models continues to increase, orthogonal loss will bring greater benefits to model convergence.

## C. Limitation

We aim to discuss the limitations herein to identify promising avenues for future exploration in this domain. To the best of our knowledge, there is no method has been shown to outperform full fine-tuning across a wide range of visual recognition tasks with extra latency. While adapter-based approaches yield impressive performance on visual tasks, they inevitably introduce extra modules and inference latency. We observe that LoRA-like methods often outperform full fine-tuning in large language models (LLMs) without incurring additional inference costs (Ding et al., 2023). This is primarily because the input and output distributions of LLMs are nearly homogeneous. LoRA excels at LLMs due to its ability to enable efficient domain transfer for homogeneous data. For visual recognition tasks, however, the input and output distributions of foundation models during pre-training (e.g., classification, unsupervised learning) differ significantly from those of downstream tasks (e.g., detection, segmentation). Thus, fine-tuning visual foundation models for downstream tasks imposes more stringent requirements on tuning methods than fine-tuning LLMs does. Going forward, research on fine-tuning for visual recognition tasks should strive toward the goal of zero inference latency—a direction that we also intend to pursue in our future work.

## D. Adapter Tuning Paradigm

For dataset  $D = \{(x_i, y_i)\}_{i=1}^N$ , fine-tuning calculates the loss between inference results and labels according to the

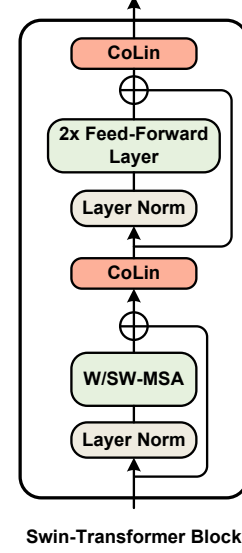


Figure 5. Insertion location. CoLin is inserted after the two skip connections in each SwinBlock.

formula:

$$L(D, \theta) = \sum_{i=1}^N \text{loss}(f_\theta(x_i), y_i),$$

where  $f_\theta$  denotes the network forward function and  $\text{loss}$  represents the loss function. After that,  $\theta$  is optimized through

$$\theta \leftarrow \arg \min_{\theta} L(D, \theta).$$

In adapter tuning paradigm, parameters consist of two parts, including parameters in adapter  $\theta_A$  and parameters in the original architecture  $\theta$ . Here,  $\theta$  is further divided into frozen part  $\theta_F$  and trainable part  $\theta_T$ , noted as  $\theta = \{\theta_F, \theta_T\}$ . Let  $\Omega$  be all the trainable parameters, then  $\Omega = \{\theta_A, \theta_T\}$ . The loss function and optimization formula in adapter can be written as:

$$L(D, \theta_F, \Omega) = \sum_{i=1}^N \text{loss}(f_{\theta_F, \Omega}(x_i), y_i),$$

$$\Omega \leftarrow \arg \min_{\Omega} L(D, \theta_F, \Omega).$$

## E. The Position of CoLin in Swin

Our experiments are conducted based on the Swin Transformer (Swin-B and Swin-L). We insert CoLin sequentially after the two skip connections following the configuration illustrated in Figure 5.